ICASSP 2024 - 2024 IEEE International Conference on Acoustics, Speech and Signal Processing (ICASSP) | 979-8-3503-4485-1/24/$31.00 ©2024 IEEE | DOI: 10.1109/ICASSP48485.2024.10447698

INTEGRATED LOCALIZATION AND COMMUNICATION IN 3GPP INDUSTRIAL ENVIRONMENTS

Girim Kwon, Zhenyu Liu*, Andrea Conti†, Hyuncheol Park‡, and Moe Z. Win**

*Wireless Information and Network Sciences Laboratory, Massachusetts Institute of Technology
†Wireless Communication and Localization Networks Laboratory, University of Ferrara
‡School of Electrical Engineering, Korea Advanced Institute of Science and Technology

ABSTRACT

Integrated localization and communication (ILC) will be a key enabler for providing accurate location information and high data rate in next generation networks. This paper proposes a transmission frame structure and a soft information (SI)-based localization algorithm for position-assisted communications. The proposed ILC achieves improved localization accuracy and enhanced communication rate simultaneously by accounting for the statistical characteristics of the wireless environment. Results in 3rd Generation Partnership Project (3GPP) industrial scenarios show that the SI-based localization algorithm can achieve decimeter-level accuracy. Moreover, the position-assisted communication enhances the achievable rate, especially in scenarios with high mobility.

Index Terms— Integrated localization and communication, next generation networks, MIMO, OFDM, soft information.

1. INTRODUCTION

Integrated localization and communication (ILC) is expected to play a key role for applications in next generation networks [1–8] including autonomy, crowd sensing, smart environments, assets tracking, and Internet-of-Things (IoT). The main challenge in designing ILC is to achieve improved localization accuracy and enhanced communication rate simultaneously with shared resources in complex wireless environments (e.g., indoor factory and urban area).

In recent years, localization in fifth generation (5G)-and-beyond networks has been explored in the literature, while research on ILC method is still lacking. The existing works are categorized into three main streams: (i) performance analysis [9, 10], (ii) transceiver design [11, 12], and (iii) localization algorithm design [13, 14]. For accurate localization and high-rate communication, harsh wireless propagation conditions (e.g., line-of-sight (LOS) blockage and multi-path scattering) should be taken into account in designing algorithms.

Classical localization techniques relying on single-value estimates (SVEs) (e.g., range and angle estimates) may suffer from performance loss as the SVEs are biased in the aforementioned harsh propagation conditions [15–17]. To overcome this drawback, the direct positioning (DP) has been proposed [18–20]. To capture richer information from heterogeneous measurements, soft information (SI)-based localization has been investigated [5, 7, 21]. SI contains all the positional information inherent in the signal measurements as well as contextual data, allowing improved inference. For a full exploitation of SI, we characterize the relationship between the received reference signals and the positions in realistic propagation environments. This allows to account for signal correlation across different frequencies of the wideband system and for cooperation in networks, thus improving localization and communication performance.

The goal of this paper is to design a method for achieving improved localization accuracy and enhanced communication rate. We advocate position-assisted communication, via a suitable ILC frame structure, in which the positions of user equipments (UEs) are simultaneously estimated and used for reducing communication overhead. The key idea is to exploit the spatial reciprocity of uplink (UL) and downlink (DL) channels, as well as the correlation among subcarriers. This paper proposes a cooperative ILC method for multiple-input multiple-output (MIMO)-orthogonal frequency division multiplexing (OFDM) networks. The proposed method significantly outperforms existing techniques in 3rd Generation Partnership Project (3GPP) industrial scenarios.[1]

Notations: A random variable (RV) and its realization are denoted by x and x for a scalar; $\mathbf{x}$ and $\boldsymbol{x}$ for a vector; $\mathbf{X}$ and $\boldsymbol{X}$ for a matrix; X and $\mathcal{X}$ for a set. $\varphi(\boldsymbol{x};\boldsymbol{\mu},\boldsymbol{\Sigma})$ is the probability distribution function (PDF) of a circularly-symmetric complex Gaussian (CSCG) RV $\mathbf{x}$ with mean $\boldsymbol{\mu}$ and covariance $\boldsymbol{\Sigma}$. $\delta_{i,j}$ is the Kronecker delta function. $\boldsymbol{X}^{\mathrm{T}}$ (or $\boldsymbol{X}^{\dagger}$) is the transpose (or conjugate transpose) of $\boldsymbol{X}$.

The fundamental research described in this paper was supported, in part, by the National Research Foundation of Korea under Grant 2021R1A6A3A14040142, by the Ministry of Science and ICT under Grant IITP-2024-RS-2023-00259991, by the Office of Naval Research under Grant N62909-22-1-2009, by the National Science Foundation under Grant CNS-2148251, and by federal agency and industry partners in the RINGS program.
Corresponding author: Moe Z. Win (e-mail: moewin@mit.edu).

[1] An extended version of this work can be found in [22].

2. SYSTEM MODEL

2.1. ILC with gNodeB Cooperation

Consider ILC for a network with $N_{\rm B}$ gNodeBs (gNBs) and $N_{\rm U}$ UEs, where each gNB and UE have $M_{\rm B}$ and $M_{\rm U}$ antennas, respectively. The gNBs cooperatively receive and transmit the signals for localization and communication, respectively. For wideband operation, MIMO-OFDM system with K subcarriers and the subcarrier spacing Δf is adopted as in 3GPP New Radio (NR). For efficient use of the frequency band and hardware system, UL localization and DL communication are incorporated as a form of ILC. To improve the performance of the ILC, gNB cooperation is adopted for macrodiversity. Since the data rate may be reduced by the overhead required for reference/pilot signal transmission and channel information feedback, an efficient ILC method is designed based on position-assisted communication.

The proposed frame structure consists of two sequential phases. The first phase is to estimate the UE positions at the gNBs using short UL reference signals, while the second phase is to transmit the pilot and data symbols in DL by exploiting the position information. In particular, the UL reference signals are transmitted simultaneously from multiple UEs in different subcarriers. Then the received signals at the gNBs are used for the SI-based localization based on statistical characterization of the OFDM signals. This is possible as the spatial information are correlated over all the subcarriers. In the DL communication phase, all the subcarriers are shared to all the UEs via space division multiple access. The channel acquisition overhead can be significantly reduced by using the estimated position information.

2.2. Channel Model

The three-dimensional (3D) positions and orientation angles of the bth gNB are denoted by $\boldsymbol{q}_b$ and $(\varphi_b^{\rm B}, \vartheta_b^{\rm B})$, respectively, which are known to all the gNBs. In particular, $\varphi_b^{\rm B}$ and $\vartheta_b^{\rm B}$ are angles with respect to the z-axis and the $-x$-axis, respectively. The uth UE is located at an unknown position $\boldsymbol{p}_u$.

For fixed $\boldsymbol{p}_u$ and $\boldsymbol{q}_b$, the UL channel from the uth UE to the bth gNB at the kth subcarrier is expressed as [23]

$$\mathsf{H}_{b,u}[k] = \chi_{b,u}\, \boldsymbol{H}_{b,u,0}[k] + \sum_{l=1}^{L-1} \mathsf{H}_{b,u,l}[k] \tag{1}$$

where $\boldsymbol{H}_{b,u,0}[k] \triangleq (M_{\rm B} M_{\rm U} \tilde{h}_{b,u}^{(\rm L)})^{\frac{1}{2}} e^{-\imath 2\pi k \Delta f \tau_{b,u}} \boldsymbol{a}_{\rm B}(\phi_{b,u}, \theta_{b,u}) \times \boldsymbol{a}_{\rm U}^{\dagger}(\phi'_{b,u}, \theta'_{b,u})$ and $\mathsf{H}_{b,u,l}[k] \triangleq (\varrho_{b,u,l} M_{\rm B} M_{\rm U} \tilde{h}_{b,u}^{(\rm N)})^{\frac{1}{2}} \alpha_{b,u,l} \times e^{-\imath 2\pi k \Delta f \tau_{b,u,l}} \boldsymbol{a}_{\rm B}(\varphi_{b,u,l}, \theta_{b,u,l}) \boldsymbol{a}_{\rm U}^{\dagger}(\varphi'_{b,u,l}, \theta'_{b,u,l})$ for the LOS and non-line-of-sight (NLOS) paths, respectively. The LOS indicator $\chi_{b,u} \in \{0,1\}$ becomes 1 with probability $p_{\rm L}(r_{b,u})$ as a function of the LOS distance $r_{b,u}$. The large-scale gains are $\tilde{h}_{b,u}^{(\rm L)} \triangleq c_{\rm L} r_{b,u}^{-\beta_{\rm L}}$ and $\tilde{h}_{b,u}^{(\rm N)} \triangleq c_{\rm N} r_{b,u}^{-\beta_{\rm N}}$ with the pathloss exponents $\beta_{\rm L}$ and $\beta_{\rm N}$; the constants $c_{\rm L}$ and $c_{\rm N}$. The propagation delays are denoted by $\tau_{b,u}$ and $\tau_{b,u,l}$, where $\tau_{b,u} = r_{b,u}/c$ with the speed of light c. The path gain $\alpha_{b,u,l}$ follows the standard CSCG distribution. The NLOS path power satisfies $\sum_{l=1}^{L-1} \varrho_{b,u,l} = 1$, where the paths can be grouped into clusters. The normalized array response vector of the gNBs is denoted by $\boldsymbol{a}_{\rm B}(\phi, \theta) \in \mathbb{C}^{M_{\rm B}}$ as a function of the azimuth and zenith angle-of-arrivals (AOAs). Similarly, $\boldsymbol{a}_{\rm U}(\phi, \theta) \in \mathbb{C}^{M_{\rm U}}$ is for the UE. Note that the AOAs and delay for the LOS can be expressed as functions of $\boldsymbol{p}_u$ for given $\boldsymbol{q}_b$ and $(\varphi_b^{\rm B}, \vartheta_b^{\rm B})$ [10].

The DL channel from the uth UE to the bth gNB is denoted by the matrix $\mathsf{H}'_{b,u}[k] \in \mathbb{C}^{M_{\rm U} \times M_{\rm B}}$ based on the spatial reciprocity with the similar method to (1).

2.3. Signaling Format

In the UL localization period, UEs simultaneously transmit a reference symbol $s = 1$ using distinguishable subsets of subcarriers to the gNBs. Since the UEs have no prior information about the channels or relative positions of the gNBs, they transmit the reference symbol through a single antenna element with the omnidirectional radiation pattern instead of a directional beam. In this case, the transmit beamforming (BF) vector of the UEs is expressed as $\boldsymbol{e}_1 \triangleq [1, 0, 0, \ldots, 0]^{\rm T}$ with length $M_{\rm U}$. Specifically, the received signal at the kth subcarrier of the bth gNB from the uth UE becomes

$$\mathsf{y}_{b,u}[k] = \sqrt{P_{\rm t}} \chi_{b,u} \boldsymbol{h}_{b,u,0}[k] s + \sum_{l=1}^{L-1} \sqrt{P_{\rm t}} \mathsf{h}_{b,u,l}[k] s + \mathsf{n}_{b,u}[k] \tag{2}$$

with $\boldsymbol{h}_{b,u,0}[k] \triangleq \left(M_{\rm B} \tilde{h}_{b,u}^{(\rm L)}\right)^{\frac{1}{2}} e^{-\imath 2\pi k \Delta f \tau_{b,u}} \boldsymbol{a}_{\rm B}(\phi_{b,u}, \theta_{b,u})$ and $\mathsf{h}_{b,u,l}[k] \triangleq \left(\varrho_{b,u,l} M_{\rm B} \tilde{h}_{b,u}^{(\rm N)}\right)^{\frac{1}{2}} \alpha_{b,u,l} e^{-\imath 2\pi k \Delta f \tau_{b,u,l}} \boldsymbol{a}_{\rm B}(\varphi_{b,u,l}, \theta_{b,u,l})$ where $k \in \mathcal{K}_u \subseteq \{1, 2, \ldots, K\}$ and $\mathcal{K}_u \cap \mathcal{K}_j = \emptyset$ for $j \neq u$. The size of $\mathcal{K}_u$ affects the localization accuracy. $P_{\rm t}$ is the transmit power of the UE. The noise vector $\mathsf{n}_{b,u}[k]$ follows the CSCG distribution, $\mathcal{CN}(\mathbf{0}, P_{\rm n} \boldsymbol{I})$ with the noise power $P_{\rm n}$.

In the DL pilot transmission period, a subset of gNBs $\mathcal{B}_u$ is associated with the uth UE based on the results of the UL localization. Then the BF matrix $\boldsymbol{F}_b \triangleq \left[\boldsymbol{f}_{b,u}, \forall u \in \mathcal{U}_b\right] \in \mathbb{C}^{M_{\rm B} \times |\mathcal{U}_b|}, \forall b$ is used at all the subcarriers to allow a low complexity channel acquisition at the UEs. The set $\mathcal{U}_b$ includes the UEs associated with the bth gNB. $\boldsymbol{F}_b$ is used for both pilot and data transmissions to reduce the pilot overhead and feedback overhead. The gNBs in $\mathcal{B}_u$ simultaneously transmit the pilot to the uth UE using each $\boldsymbol{f}_{b,u} \in \mathbb{C}^{M_{\rm B}}$. The details are in Sec. 4. In the DL data transmission period, gNBs cooperatively transmit the symbols to the UEs for given effective channels without channel state information (CSI) feedback. The combined signal at the uth UE for data transmission is

$$\mathsf{y}'_u[k] = \boldsymbol{w}_u^{\dagger} \sum_{b=1}^{N_{\rm B}} \sqrt{P'_{\rm t}/|\mathcal{U}_b|}\, \boldsymbol{H}'_{b,u}[k] \boldsymbol{F}_b \mathsf{d}_b[k] + \boldsymbol{w}_u^{\dagger} \mathsf{n}'_u[k] \tag{3}$$

where $\boldsymbol{w}_u \in \mathbb{C}^{M_{\rm U}}$ is the receive BF vector, and $P'_{\rm t}$ is the transmit power of the gNB. The data symbol vector is denoted by $\mathsf{d}_b[k] = [\mathsf{s}'_j[k], j \in \mathcal{U}_b]^{\rm T}$, where $\mathsf{s}'_j[k]$ corresponds to the jth UE. The power normalization satisfies $\mathbb{E}\left\{\mathsf{d}_b[k](\mathsf{d}_b[m])^{\dagger}\right\} = \frac{1}{|\mathcal{U}_b|} \delta_{k,m} \boldsymbol{I}_{|\mathcal{U}_b|}$ and $\|\boldsymbol{F}_b\|_{\rm F}^2 = |\mathcal{U}_b|$. The noise at the UE follows $\mathsf{n}'_u[k] \sim \mathcal{CN}(\mathbf{0}, P'_{\rm n} \boldsymbol{I})$ with the power $P'_{\rm n}$.

3. SI-BASED LOCALIZATION ALGORITHM

3.1. SI-based Localization with Approximate Maximum Likelihood Estimation

For notational brevity, it is assumed that the subcarriers $k = 1, 2, \dots, K$ are used for localization of the uth UE. We aim to estimate $\boldsymbol{p}_u$ by observing $\bar{\boldsymbol{y}}_{b,u}[K] = [\boldsymbol{y}_{b,u}^{\mathrm{T}}[K], \boldsymbol{y}_{b,u}^{\mathrm{T}}[K-1], \dots, \boldsymbol{y}_{b,u}^{\mathrm{T}}[1]]^{\mathrm{T}}$. Since all positional information can be captured by the SI associated with statistical models used in (2), the maximum likelihood (ML) estimation is considered as

$$\mathscr{P}_0: \ \hat{\boldsymbol{p}}_u = \underset{\boldsymbol{p}_u}{\operatorname{argmax}} \sum_{b=1}^{N_{\mathrm{B}}} \log f\big(\bar{\boldsymbol{y}}_{b,u}[K]; \boldsymbol{p}_u\big)$$

where $f\big(\bar{\boldsymbol{y}}_{b,u}[K]; \boldsymbol{p}_u\big)$ is the PDF of $\bar{\mathbf{y}}_{b,u}[K]$ for a given $\boldsymbol{p}_u$.

To solve $\mathscr{P}_0$, the joint PDF of $\bar{\mathbf{y}}_{b,u}[K]$ is derived using a Gaussian approximation and a factorization method as $f\big(\bar{\boldsymbol{y}}_{b,u}[K]; \boldsymbol{p}_u\big) \approx p_{\mathrm{L}}(r_{b,u}) \prod_{k=1}^{K-1} \tilde{\varphi}_{b,u}^{(1)}[k] + \big(1 - p_{\mathrm{L}}(r_{b,u})\big) \times \prod_{k=1}^{K-1} \tilde{\varphi}_{b,u}^{(0)}[k]$ with $\tilde{\varphi}_{b,u}^{(\chi)}[k] \triangleq \varphi\big(\boldsymbol{y}_{b,u}[k]; \tilde{\boldsymbol{\mu}}_{b,u}^{(\chi)}[k], \tilde{\boldsymbol{\Sigma}}_{b,u}[k]\big)$. The detailed derivation and the definitions are given in [22].

3.2. Expectation-Maximization Algorithm

$\mathscr{P}_0$ is still difficult to solve due to the complicated PDF expression. To resolve this, the concept of *complete data* is introduced, instead of relying only on the observed data.

Define the random set $\mathsf{Z}_{b,u} \triangleq \big\{\bar{\mathbf{y}}_{b,u}[K], \chi_{b,u}\big\}$ as *complete data*, including both the observed data $\bar{\mathbf{y}}_{b,u}[K]$ and the unobserved data $\chi_{b,u}$. The PDF of $\mathsf{Z}_{b,u}$ can be expressed as $f\big(\mathcal{Z}_{b,u}; \boldsymbol{p}_u\big) = f\big(\chi_{b,u}; \boldsymbol{p}_u\big) f\big(\bar{\boldsymbol{y}}_{b,u}[K] \big| \chi_{b,u}; \boldsymbol{p}_u\big) \approx \big[p_{\mathrm{L}}(r_{b,u}) \prod_{k=1}^{K} \tilde{\varphi}_{b,u}^{(1)}[k]\big]^{\chi_{b,u}} \big[\big(1 - p_{\mathrm{L}}(r_{b,u})\big) \prod_{k=1}^{K} \tilde{\varphi}_{b,u}^{(0)}[k]\big]^{1-\chi_{b,u}}$ where $f\big(\chi_{b,u}; \boldsymbol{p}_u\big) = \big(p_{\mathrm{L}}(r_{b,u})\big)^{\chi_{b,u}} \big(1 - p_{\mathrm{L}}(r_{b,u})\big)^{1-\chi_{b,u}}$.

Since the complete data cannot be fully observed, the algorithm maximizes the expected log-likelihood such that

$$\mathscr{P}_1: \ \hat{\boldsymbol{p}}_u = \underset{\boldsymbol{p}_u}{\operatorname{argmax}} \, \mathbb{E}_{\chi_{b,u}} \Big\{ \sum_{b=1}^{N_{\mathrm{B}}} \ln f\big(\mathsf{Z}_{b,u}; \boldsymbol{p}_u\big) \Big| \bar{\boldsymbol{y}}_{b,u}[K] \Big\}$$

where the expectation is taken over the following distribution,

$$f\big(\chi_{b,u} \big| \bar{\boldsymbol{y}}_{b,u}[K]; \boldsymbol{p}_u\big) = f\big(\mathcal{Z}_{b,u}; \boldsymbol{p}_u\big) / f\big(\bar{\boldsymbol{y}}_{b,u}[K]; \boldsymbol{p}_u\big). \quad (4)$$

Algorithm 1 proceeds in multiple iterations including inner iterations, where each outer iteration consists of an expectation step and a maximization step. For the expectation step in the tth outer iteration, (4) is evaluated for given $\boldsymbol{p}_u^{(t-1)}$ from the $(t-1)$th iteration. Then the expected log-likelihood of $\mathsf{Z}_{b,u}$ is evaluated as $\ell_u\big(\boldsymbol{p}_u; \boldsymbol{p}_u^{(t-1)}\big) \triangleq \sum_{b=1}^{N_{\mathrm{B}}} \sum_{\chi_{b,u} \in \{0,1\}} f\big(\chi_{b,u} \big| \bar{\boldsymbol{y}}_{b,u}[K]; \boldsymbol{p}_u^{(t-1)}\big) \ln f\big(\mathcal{Z}_{b,u}; \boldsymbol{p}_u\big)$. Next, perform the maximization step: $\boldsymbol{p}_u^{(t)} = \operatorname{argmax}_{\boldsymbol{p}_u} \ell_u\big(\boldsymbol{p}_u; \boldsymbol{p}_u^{(t-1)}\big)$. Since $\ell_u\big(\boldsymbol{p}_u; \boldsymbol{p}_u^{(t-1)}\big)$ is twice differentiable with respect to $\boldsymbol{p}_u$, a local optimal point is found by a modified Newton's method using the gradient $\nabla \ell_u = \frac{\partial \ell_u}{\partial \boldsymbol{p}_u} \in \mathbb{R}^{3 \times 1}$ and Hessian matrix $\nabla^2 \ell_u = \frac{\partial}{\partial \boldsymbol{p}_u} (\nabla \ell_u)^{\mathrm{T}} \in \mathbb{R}^{3 \times 3}$ as in the lines 10–17.

Algorithm 1 Expectation-maximization algorithm for localization of the uth UE

Require: $\{\bar{\boldsymbol{y}}_{b,u}[K], \boldsymbol{q}_b, \varphi_b^{\mathrm{B}}, \vartheta_b^{\mathrm{B}}, b = 1, 2, \dots, N_{\mathrm{B}}\}, P_{\mathrm{n}}, P_{\mathrm{t}}$
1: $\epsilon \leftarrow$ a small positive number, and $t \leftarrow 0$
2: Initialize $\boldsymbol{p}_u^{(t)}$ with a random position
3: **while** $\boldsymbol{p}_u^{(t)}$ does not converge within max iteration **do**
4: $\quad t \leftarrow t + 1$
5: $\quad$ Calculate $f\big(\chi_{b,u} \big| \bar{\boldsymbol{y}}_{b,u}[K]; \boldsymbol{p}_u^{(t-1)}\big), \forall \chi_{b,u}$ using (4)
6: $\quad s \leftarrow 0$
7: $\quad \boldsymbol{p}_u^{(t,s)} \leftarrow \boldsymbol{p}_u^{(t-1)}$
8: $\quad$ **while** $\boldsymbol{p}_u^{(t,s)}$ does not converge **do**
9: $\qquad s \leftarrow s + 1$
10: $\qquad$ **if** $\nabla^2 \ell_u$ is negative definite **then**
11: $\qquad\quad \boldsymbol{D}_u^{(t,s)} \leftarrow \big(\nabla^2 \ell_u\big)^{-1}$
12: $\qquad$ **else**
13: $\qquad\quad \lambda \leftarrow$ the smallest eigenvalue of $-\nabla^2 \ell_u$
14: $\qquad\quad$ Find $\gamma^{(t,s)}$ by backtracking line search
15: $\qquad\quad \boldsymbol{D}_u^{(t,s)} \leftarrow \gamma^{(t,s)} \big(\nabla^2 \ell_u - (|\lambda| + \epsilon) \boldsymbol{I}\big)^{-1}$
16: $\qquad$ **end if**
17: $\qquad \boldsymbol{p}_u^{(t,s)} \leftarrow \boldsymbol{p}_u^{(t,s-1)} - \boldsymbol{D}_u^{(t,s)} \nabla \ell_u\big(\boldsymbol{p}_u^{(t,s-1)}; \boldsymbol{p}_u^{(t-1)}\big)$
18: $\quad$ **end while**
19: $\quad \boldsymbol{p}_u^{(t)} \leftarrow \boldsymbol{p}_u^{(t,s)}$
20: **end while**
21: $\hat{\boldsymbol{p}}_u \leftarrow \boldsymbol{p}_u^{(t)}$
Return: $\hat{\boldsymbol{p}}_u$

4. POSITION-ASSISTED COMMUNICATION

4.1. UE Association and Transmit Beamforming

The overhead for channel acquisition and feedback for DL communication is reduced by determining $\mathcal{U}_b$ and $\boldsymbol{F}_b$ from the results of localization. First, the LOS existence is detected by comparing the conditional probability mass function (PMF) values in (4) as $\widehat{\chi}_{b,u} = \operatorname{argmax}_{\chi_{b,u} \in \{0,1\}} f\big(\chi_{b,u} \big| \bar{\boldsymbol{y}}_{b,u}[K]; \hat{\boldsymbol{p}}_u\big)$. Then determine the set $\mathcal{U}_b$ that contains the UEs having the LOS path from the bth gNB as well as the BF matrix $\boldsymbol{F}_b$ as $\mathcal{U}_b = \big\{u : u \in \{1, 2, \dots, N_{\mathrm{U}}\}$ and $\widehat{\chi}_{b,u} = 1\big\}$ and $\boldsymbol{F}_b = \big[\boldsymbol{f}_{b,u}, \forall u \in \mathcal{U}_b\big]$ with $\boldsymbol{f}_{b,u} = \boldsymbol{a}_{\mathrm{B}}\big(\hat{\phi}_{b,u}, \hat{\theta}_{b,u}\big)$ where $\hat{\phi}_{b,u}$ and $\hat{\theta}_{b,u}$ are obtained from converting $\hat{\boldsymbol{p}}_u$. The more accurate the position estimation, the higher communication rate can be achieved as the beam direction of $\boldsymbol{f}_{b,u}$ becomes more accurate to the uth UE. $\boldsymbol{F}_b$ is also used for data transmission without any CSI feedback from UEs. In summary, both the pilot and feedback overheads are significantly reduced by using the position-assisted UE association and BF.

4.2. Receive Beamforming

The receive BF vector for the kth subcarrier at the uth UE is denoted by $\boldsymbol{w}_u[k]$. Using $\mathcal{U}_b$ and $\boldsymbol{F}_b$, the corresponding signal-to-interference-plus-noise ratio (SINR) is expressed as

$$\gamma_u[k] = \frac{\boldsymbol{w}_u^{\dagger}[k] \Big(\boldsymbol{h}_{u,u}^{\mathrm{eff}}[k] \big(\boldsymbol{h}_{u,u}^{\mathrm{eff}}[k]\big)^{\dagger} \Big) \boldsymbol{w}_u[k]}{\boldsymbol{w}_u^{\dagger}[k] \Big(\sum_{\substack{j=1, \\ j \neq u}}^{N_{\mathrm{U}}} \boldsymbol{h}_{u,j}^{\mathrm{eff}}[k] \big(\boldsymbol{h}_{u,j}^{\mathrm{eff}}[k]\big)^{\dagger} + P_{\mathrm{n}}' \boldsymbol{I} \Big) \boldsymbol{w}_u[k]}. \quad (5)$$

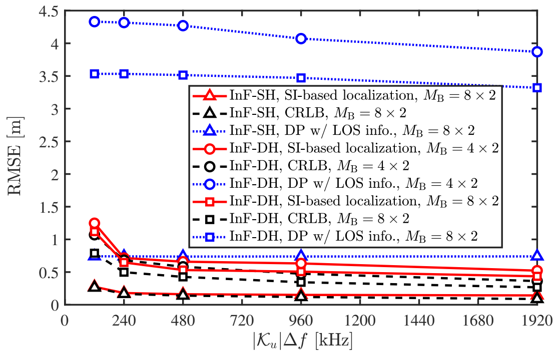

Fig. 1. Position error for different bandwidths: $|\mathcal{K}_u|$ is the number of subcarriers allocated to the UE.

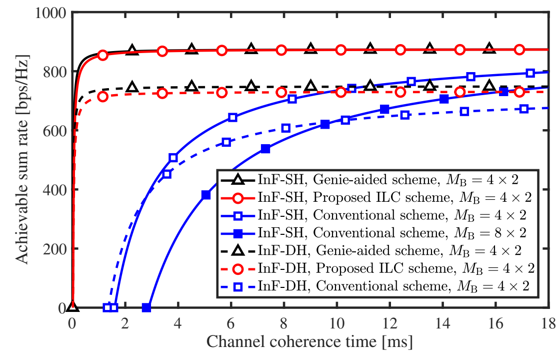

Fig. 2. Communication rate for different channel coherence times: $N_U = 2$, $M_U = 2\times2$, $K = 16$, $|\mathcal{K}_u| = 8, \forall u$, $\mu_f = 1/16$.

where $\mathcal{B}_j \triangleq \{b : b \in \{1, 2, \ldots, N_B\}$ and $j \in \mathcal{U}_b\}$ and $\boldsymbol{h}^{\text{eff}}_{u,j}[k] \triangleq \sum_{b\in\mathcal{B}_j} \sqrt{P'_t/|\mathcal{U}_b|}\boldsymbol{H}'_{b,u}[k]\boldsymbol{f}_{b,j}$. If $\mathcal{B}_u = \emptyset$, $\gamma_u[k]$ is given as zero. The vector $\boldsymbol{w}_u[k]$ is optimized by solving $\max_{\boldsymbol{w}_u[k]} \gamma_u[k]$, known as the generalized Rayleigh quotient problem [24]. Therefore, the uth UE only needs to obtain the knowledge of the aggregated effective CSI $\boldsymbol{h}^{\text{eff}}_{u,j}[k], \forall j$. This allows for a further reduction in pilot overhead such that the gNBs in $\mathcal{B}_u$ simultaneously transmit the pilot signal for each u. Then the required pilot overhead is $T_p = N_U T_s$, where T_s is the OFDM symbol period. Since T_p is independent of N_B or M_B, the position-assisted communication is more beneficial in densely deployed networks with large antenna arrays.

4.3. Achievable Communication Rate

The achievable sum rate for a given channel realization is given by the following general expression $R = \left(1 - \frac{T_u+T_p+T_f}{T_c}\right)\sum_{k=1}^{K}\sum_{u=1}^{N_U}\log_2\left(1+\gamma_u[k]\right)$ where T_u is the overhead for transmitting the reference symbols for UL localization. T_p is the pilot overhead for estimating the DL channels. T_f is the channel feedback overhead. T_c is the channel coherence time. All the UEs occupy all the subcarriers via space division multiple access in DL communications. The proposed position-assisted communication can significantly reduce T_p and T_f by using only a short T_u for localization.

5. SIMULATION RESULTS

We quantify the performance gain offered by the proposed method in 3GPP InF-SH and InF-DH scenarios for industrial IoT use cases [6, 23]. $N_B = 18$ gNBs are placed on a two-dimensional grid with 20 m spacing in a room with size 120 m×60 m×10 m [6]. The carrier frequency is 28 GHz with $\Delta f = 120$ kHz. The antenna heights are 8 m for gNBs and 1.5 m for UEs. The noise figures are 7 dB at gNBs and 13 dB at UEs. The transmit power is set as $P_t = P'_t = 23$ dBm. The uniform planar arrays of the nodes are assumed to be placed on yz-plane with zero orientation angle. The specific parameters and models for channel realizations can be found in [23].

In Fig. 1, the root-mean-square error (RMSE) of position estimate is evaluated for different localization algorithms. For comparison, the Cramér-Rao lower bound (CRLB) derived in [22] is plotted as theoretical limits. The conventional DP in [18] is also compared assuming the perfectly known $\chi_{b,u}$, where the grid resolution is set to be 0.01 m. We see that the proposed algorithm achieves decimeter-level accuracy, while approaching the theoretical limits. Note that Algorithm 1 converges within less than 10 iterations in our simulations.

In Fig. 2, the achievable rate is evaluated for different T_c. We compare with the genie-aided communication having perfect knowledge of $\boldsymbol{p}_u$ and $\chi_{b,u}$, constituting $\boldsymbol{F}_b$ with the exact information. This scheme requires the overhead of $T_u = 0$, $T_p = N_U T_s$, and $T_f = 0$. We also compare with the conventional scheme relying on DL channel estimation with $T_p = N_B M_B T_s$. In this scheme, the perfect knowledge of LOS indicator and angles are assumed to be fed back to each gNB for determining $\boldsymbol{F}_b$, for which the overhead is given by $T_f = \mu_f B_f T_s$ with the conversion factor μ_f in symbols/bit and the feedback amount $B_f = N_U N_B + 2Q\sum_{u=1}^{N_U}|\mathcal{B}_u|$ in bits. We consider $Q = 8$ bits without any quantization error. Meanwhile, the proposed scheme uses only one symbol period for UL localization, i.e., $T_u = T_s$, while the DL communication requires $T_p = N_U T_s$ and $T_f = 0$. The proposed scheme significantly outperforms the conventional scheme. It is beneficial particularly in short T_c regime, meaning that the proposed ILC can play a key role in rapidly changing environments. It also approaches the genie-aided scheme due to the high localization accuracy with the small overhead.

6. CONCLUSION

This paper developed a cooperative ILC method for MIMO-OFDM networks. In particular, an efficient ILC frame structure was proposed for position-assisted communications. By characterizing the statistical relationship between the received signals and positions, a SI-based localization algorithm was designed. Results in 3GPP indoor factory scenarios show that the proposed localization algorithm achieves decimeter-level accuracy and approaches the theoretical limits using only a short reference signal in complex wireless environments. This allows to achieve a higher communication rate without channel feedback, benefitting networks with mobility.

7. REFERENCES

[1] 3GPP Tech. Spec. Group Services System Aspects, “Service requirements for the 5G system; Stage 1 (Release 19),” TS 22.261 (V19.1.0), Dec. 2022.

[2] A. Conti, F. Morselli, Z. Liu, S. Bartoletti, S. Mazuelas, W. C. Lindsey, and M. Z. Win, “Location awareness in beyond 5G networks,” *IEEE Commun. Mag.*, vol. 59, no. 11, pp. 22–27, Nov. 2021.

[3] M. Z. Win, Y. Shen, and W. Dai, “A theoretical foundation of network localization and navigation,” *Proc. IEEE*, vol. 106, no. 7, pp. 1136–1165, Jul. 2018.

[4] 3GPP Tech. Spec. Group Radio Access Netw., “Study on NR positioning support (Release 16),” TR 38.855 (V16.0.0), Mar. 2019.

[5] F. Morselli, S. M. Razavi, M. Z. Win, and A. Conti, “Soft information based localization for 5G networks and beyond,” *IEEE Trans. Wireless Commun.*, vol. 22, no. 12, pp. 9923–9938, Dec. 2023.

[6] 3GPP Tech. Spec. Group Radio Access Netw., “Study on NR positioning Enhancements (Release 17),” TR 38.857 (V17.0.0), Mar. 2021.

[7] G. Torsoli, M. Z. Win, and A. Conti, “Blockage intelligence in complex environments for beyond 5G localization,” *IEEE J. Sel. Areas Commun.*, vol. 41, no. 6, pp. 1688–1701, Jun. 2023.

[8] S. Zeb, A. Mahmood, S. A. Hassan, M. Gidlund, and M. Guizani, “Analysis of beyond 5G integrated communication and ranging services under indoor 3-D mmwave stochastic channels,” *IEEE Trans. Ind. Informat.*, vol. 18, no. 10, pp. 7128–7138, Oct. 2022.

[9] A. Kakkavas, M. H. Castaneda Garcia, R. A. Stirling-Gallacher, and J. A. Nossek, “Performance limits of single-anchor millimeter-wave positioning,” *IEEE Trans. Wireless Commun.*, vol. 18, no. 11, pp. 5196–5210, Nov. 2019.

[10] Z. Abu-Shaban, X. Zhou, T. Abhayapala, G. Seco-Granados, and H. Wymeersch, “Error bounds for uplink and downlink 3D localization in 5G millimeter wave systems,” *IEEE Trans. Wireless Commun.*, vol. 17, no. 8, pp. 4939–4954, Aug. 2018.

[11] G. Kwon, A. Conti, H. Park, and M. Z. Win, “Joint communication and localization in millimeter wave networks,” *IEEE J. Sel. Topics Signal Process.*, vol. 15, no. 6, pp. 1439–1454, Nov. 2021.

[12] M. F. Keskin, F. Jiang, F. Munier, G. Seco-Granados, and H. Wymeersch, “Optimal spatial signal design for mmwave positioning under imperfect synchronization,” *IEEE Trans. Veh. Technol.*, vol. 71, no. 5, pp. 5558–5563, May 2022.

[13] Z. Lin, T. Lv, and P. T. Mathiopoulos, “3-D indoor positioning for millimeter-wave massive MIMO systems,” *IEEE Trans. Commun.*, vol. 66, no. 6, pp. 2472–2486, Jun. 2018.

[14] J. Palacios, G. Bielsa, P. Casari, and J. Widmer, “Single- and multiple-access point indoor localization for millimeter-wave networks,” *IEEE Trans. Wireless Commun.*, vol. 18, no. 3, pp. 1927–1942, Mar. 2019.

[15] D. Dardari, A. Conti, U. J. Ferner, A. Giorgetti, and M. Z. Win, “Ranging with ultrawide bandwidth signals in multipath environments,” *Proc. IEEE*, vol. 97, no. 2, pp. 404–426, Feb. 2009.

[16] L. Cong and W. Zhuang, “Hybrid TDOA/AOA mobile user location for wideband CDMA cellular systems,” *IEEE Trans. Wireless Commun.*, vol. 1, no. 3, pp. 439–447, Jul. 2002.

[17] U. A. Khan, S. Kar, and J. M. F. Moura, “DILAND: An algorithm for distributed sensor localization with noisy distance measurements,” *IEEE Trans. Signal Process.*, vol. 58, no. 3, pp. 1940–1947, Mar. 2010.

[18] A. J. Weiss, “Direct position determination of narrowband radio frequency transmitters,” *IEEE Signal Process. Lett.*, vol. 11, no. 5, pp. 513–516, May 2004.

[19] N. Vankayalapati, S. Kay, and Q. Ding, “TDOA based direct positioning maximum likelihood estimator and the Cramer-Rao bound,” *IEEE Trans. Aerosp. Electron. Syst.*, vol. 50, no. 3, pp. 1616–1635, Jul. 2014.

[20] O. Bialer, D. Raphaeli, and A. J. Weiss, “Maximum-likelihood direct position estimation in dense multipath,” *IEEE Trans. Veh. Technol.*, vol. 62, no. 5, pp. 2069–2079, Jun. 2013.

[21] A. Conti, S. Mazuelas, S. Bartoletti, W. C. Lindsey, and M. Z. Win, “Soft information for localization-of-things,” *Proc. IEEE*, vol. 107, no. 11, pp. 2240–2264, Nov. 2019.

[22] G. Kwon, Z. Liu, A. Conti, H. Park, and M. Z. Win, “Integrated localization and communication for efficient millimeter wave networks,” *IEEE J. Sel. Areas Commun.*, vol. 41, no. 12, pp. 3925–3941, Dec. 2023.

[23] 3GPP Tech. Spec. Group Radio Access Netw., “Study on channel model for frequencies from 0.5 to 100 GHz (Release 16),” TR 38.901 (V16.1.0), Dec. 2019.

[24] G. Golub and C. V. Loan, *Matrix Computations*, 3rd ed. Baltimore, MD: The Johns Hopkins Univ. Press, 1996.